Proc. Natl. Acad. Sci. USA
Vol. 95, pp. 6134–6138, May 1998
Cell Biology

Visualization of elongation factor G on the *Escherichia coli* 70S ribosome: The mechanism of translocation

RAJENDRA K. AGRAWAL*, PAWEL PENCZEK*†, ROBERT A. GRASSUCCI*, AND JOACHIM FRANK*†‡

*Wadsworth Center, New York State Department of Health and †Department of Biomedical Sciences, State University of New York at Albany, Empire State Plaza, Albany, NY 12201-0509

Communicated by Peter B. Moore, Yale University, New Haven, CT, March 30, 1998 (received for review March 11, 1998)

ABSTRACT **During protein synthesis, elongation factor G (EF-G) binds to the ribosome and promotes the step of translocation, a process in which tRNA moves from the A to the P site of the ribosome and the mRNA is advanced by one codon. By using three-dimensional cryo-electron microscopy, we have visualized EF-G in a ribosome–EF-G–GDP–fusidic acid complex. Fitting the crystal structure of EF-G–GDP into the cryo density map reveals a large conformational change mainly associated with domain IV, the domain that mimics the shape of the anticodon arm of the tRNA in the structurally homologous ternary complex of Phe-tRNA^{Phe}, EF-Tu, and a GTP analog. The tip portion of this domain is found in a position that overlaps the anticodon arm of the A-site tRNA, whose position in the ribosome is known from a study of the pretranslocational complex, implying that EF-G displaces the A-site tRNA to the P site by physical interaction with the anticodon arm.**

The elongation cycle of prokaryotic protein synthesis on the ribosome involves two elongation factors (EFs), EF-Tu and EF-G. EF-Tu delivers aminoacyl tRNA to the A site of the elongating ribosome, as part of the aminoacyl-tRNA–EF-Tu–GTP ternary complex, and EF-G promotes the translocation step, in which the A- and P-site tRNAs move to the P and E sites, respectively, and mRNA is advanced by one codon. Both EF-related events are accompanied by GTP hydrolysis. Furthermore, the intrinsic GTPase activity of both EF-Tu–GTP and EF-G–GTP is stimulated by the empty ribosome (1, 2) and by the tRNA-bound ribosome (3, 4). Whether the energy liberated in GTP hydrolysis is used directly for tRNA binding and translocation or for the release of the factors is not well understood. However, in a recent study, it has been proposed that it is the hydrolysis of GTP by EF-G that drives the translocation step (5).

In the present study, we present the three-dimensional (3D) binding position of the EF-G on the *Escherichia coli* 70S ribosome. Earlier immunoelectron microscopic (6) and chemical cross-linking (7) studies suggested that EF-G interacts with both subunits (30S and 50S) of the ribosome. These studies also suggested the tentative binding position of the EF-G on the ribosome. We have obtained a 3D cryo-electron microscopy map of the ribosome–EF-G–GDP–fusidic acid complex at 20-Å resolution and inferred the precise location of EF-G on the ribosome. To stablilize the ribosome–EF-G complex for cryo-electron microscopy, we used fusidic acid, an inhibitor of the translational elongation cycle that binds to the ribosome–EF-G–GDP complex and prevents the dissociation of EF-G from the ribosome (8). Because of its high occupancy, EF-G is directly visible in our 3D cryo map. A detailed comparison of the cryo electron microscopy mass attributable to EF-G with the crystal structure of EF-G–GDP (9, 10) reveals the 3D interaction sites between the ribosome and the various domains of the EF-G. Most interesting is the observation that the position of domain IV of the EF-G overlaps with the anticodon arm of the A-site tRNA (11, 12).

MATERIALS AND METHODS

Tight-coupled 70S ribosomes from *E. coli* MRE 600 and EF-G from its 100,000 × *g* supernatant were isolated as described by Burma *et al.* (13), except that the EF-G preparation was subjected to one additional step of purification by size-exclusion chromatography on Sephacryl S-200 (Sigma). The homogeneity of EF-G preparation was checked by PAGE. Both ribosomes and EF-G preparations were dialyzed in buffer containing 20 mM Tris·HCl (pH 7.5), 6 mM $MgCl_2$, 150 mM NH_4Cl, 2 mM spermidine, 0.4 mM spermine, and 5 mM 2-mercaptoethanol. The ribosome–EF-G–GDP–fusidic acid complex was prepared in 100 μl of the same buffer by incubating activated 70S ribosomes (0.032 μM) with EF-G (0.8 μM) and GTP (15 μM) at 37°C for 7 min and continuing the reaction for another 5 min after the addition of fusidic acid (0.5 mM). The complex was immediately applied to the electron microscope grid for cryo grid preparation and electron microscopy.

Micrographs were recorded as two defocus groups, at 1.67 μm and 1.00 μm, by using the low-dose protocol (10 $e^-/Å^2$) on a Philips EM420, equipped with low-dose kit and a GATAN (model 626) cryo transfer holder, at a magnification of ×52,200 (±2%) as checked by a tobacco mosaic virus standard. Micrographs were checked for drift, astigmatism, and the presence of Thon rings by optical diffraction and scanned on a Perkin–Elmer PDS 1010A microdensitometer with a step size of 25 μm corresponding to 4.78 Å on the object scale. For 3D reconstruction, a total of 3,237 ribosomes in the 1.67-μm group and 4,326 ribosomes in the 1.00-μm group were selected from a total of 25 micrographs by an automated selection procedure (14), and particle candidates were directly compared with the reference set of 87 quasi-evenly spaced projections (15) of an existing best-resolution reconstruction. For each defocus group, one step of the 3D projection alignment procedure (15) was applied and the merged contrast transfer function (CTF)-corrected structure was computed as described (16). Starting each time with the CTF-modified reconstruction of the previous step, this refinement was repeated five times with a 2.0° angular step. The final resolution was 20 Å as estimated with the Fourier shell correlation with a cutoff value of 0.5 (17). The occupancy of EF-G was estimated by comparing the average densities within L1 protein regions with the region corresponding to EF-G. By using as a reference the known density of the surrounding ice, the EF-G occupancy was calculated as ≈96%. The region corresponding to EF-G was

The publication costs of this article were defrayed in part by page charge payment. This article must therefore be hereby marked "*advertisement*" in accordance with 18 U.S.C. §1734 solely to indicate this fact.

© 1998 by The National Academy of Sciences 0027-8424/98/956134-5$2.00/0
PNAS is available online at http://www.pnas.org.

Abbreviations: EF, elongation factor; 3D, three-dimensional.

‡To whom reprint requests should be addressed. e-mail: joachim@wadsworth.org.

separated by using the envelope of the 70S ribosome without EF-G.

To check the reproducibility of the reconstruction, we made an attempt to compute two maximally dissimilar structures derived from the same data set. We divided the available set of ribosome images into halves based on the values of the cross-correlation coefficient between the experimental images and projections of the reconstruction. For the two subsets we calculated the corresponding 3D volumes, which served as seeds in an iterative procedure in which the ribosome projections were dynamically reassigned to one of two possible classes based on their similarity to the updated volumes. After reaching a stable projection assignment the two final volumes were compared and it was verified that the density mass interpreted as domain IV occupied the same position, within an angstrom. The bias in these two reconstructions revealed itself in a number of minor differences in the overall density distribution, but none have any impact on the conclusions about the domain's positions.

RESULTS AND DISCUSSION

Because of the high (>95%) occupancy of the EF-G, it is directly visible in our 3D cryo map (Fig. 1). Five sites of interaction with the ribosome are observed: three on the 50S subunit, all located on the base of the L7/L12 stalk, and two sites on the 30S subunit, at the junction of the platform and neck and in a region on the lower body. Most notable is the binding position of an arm-like structure in the neck region, at the origin of the platform, near the anticodon binding region of the A-site tRNA (11, 12).

Comparison of the x-ray structure of the EF-G–GDP complex of *Thermus thermophilus* (9, 10), which consists of five domains (numbered I–V: domain I is presented as two subdomains, the GTP binding core G domain and an insert G′ domain; see ref. 10), to the density mass attributable to EF-G shows a close match in overall size and shape (Fig. 2) and reveals a significant conformational change of EF-G in the ribosome-bound state. Domain IV, in conjunction with domains III and V, represents a substructure that mimics the tRNA portion of the ternary complex (19). By itself, domain IV with its elongate shape mimics the anticodon arm of tRNA (19).

We took three approaches in an attempt to obtain the best fit of the x-ray structure (9) into the EF-G density map: (*i*) by aligning the x-ray structure into the density map to achieve a best overall fit (because the EF-G visible in the density map is elongated compared with its x-ray structure, this approach gives a poor fit, with a cross-correlation value of 0.72); (*ii*) by using domains I and II of the x-ray structure as the main guide, which leads to serious misalignment in the arm-like region associated with domain IV (Fig. 2*A*) and decreases the cross-correlation value to 0.67; and (*iii*) by keeping domains I and II at the same position, as obtained from the second approach, but moving an entire substructure formed by domains III–V (Fig. 2*B*). This third approach yields a cross-correlation value of 0.81 and thus provides the best explanation of the density map. Although the structure of domain III is only partially defined by x-ray crystallography (see ref. 20), the structure obtained by modeling (9) fits very well into our EF-G density map (Fig. 2*B*).

Sequence analysis of EF-G from fusidic acid-resistant mutants (21) shows that amino acid residues responsible for fusidic acid binding are present in the GTP binding core G domain, as well as in domains III and V. The variant of the EF-G–GDP structure obtained by the joint fitting of domains III–V into the cryo map (Fig. 2*B*) may represent a transient conformation of the ribosome-bound factor that follows GTP hydrolysis and is prevented from assuming the conformation of the unbound factor by the binding of fusidic acid. It is also possible that the crystal structure, because of involvement of crystal packing forces, represents a nonphysiological conformation of EF-G (9). The structure of the GTP form of EF-G and the way it might be affected by GTP hydrolysis in the ribosome-bound state are unknown. However, a conformational change corresponding to that seen between the GTP and GDP forms of EF-Tu (22) does not appear to take place in the case of unbound EF-G (20).

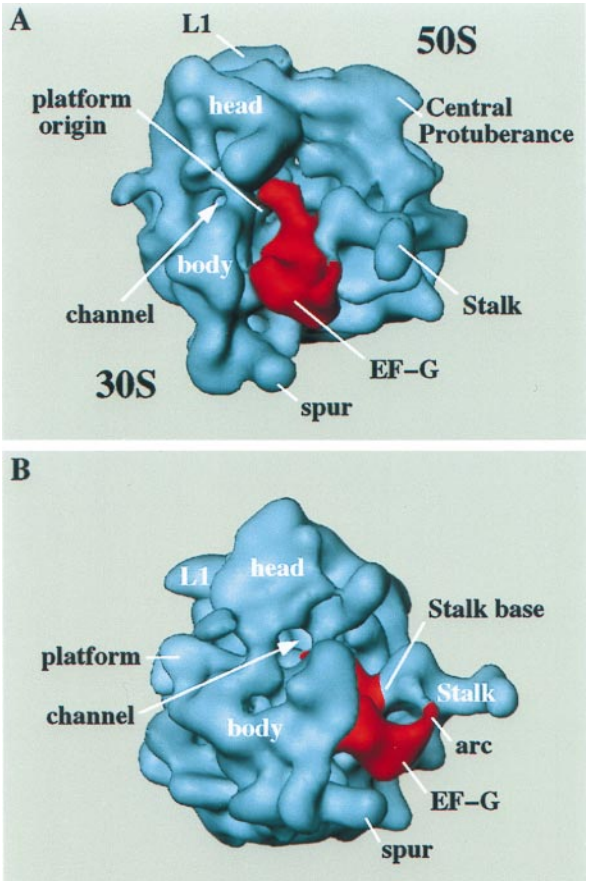

FIG. 1. The 3D cryo electron microscope maps of *E. coli* 70S ribosome complexed with EF-G–GDP–fusidic acid. (*A*) Side view showing the binding position of EF-G (red) in the intersubunit space. The 30S subunit is on the left and 50S subunit is on the right. EF-G is directly visible and seen to interact with both 30S and 50S subunits (6, 7). The tip of the elongated portion of EF-G is situated in the neck region of 30S subunit, where the anticodon loop region of A site tRNA binds (11, 12). (*B*) The 30S side view, showing the arc-like structure formed between the EF-G and a protusion at the base of the L7/L12 stalk. Note the clearly defined well-extended L7/L12 stalk. In this view, the tip (domain IV) of EF-G can be seen through the 30S channel (18) where the anticodon of A site tRNA in a pretranslocational complex binds (ref 12; R.K.A., P.P., R.A.G., N. Burkhardt, R. Jünemann, K. H. Nierhaus, and J.F., unpublished results; also see Fig. 4). Landmarks: L1, protein L1 of the 50S subunit; arc, arc-like connection between EF-G and an extension from the stalk base (see text).

The fit between the x-ray structure and the density map attributable to EF-G (Fig. 2*B*) shows that the tip of domain IV makes contact with the inner edge of the origin of the platform in the immediate vicinity of the proposed mRNA channel (18) and in close proximity to the head of the 30S subunit. This is the region where the anticodon arm of the A site tRNA is situated (11, 12). EF-G is known to form a cross-link with the S19 protein (7), which is mapped in the head region of the 30S subunit (23), and it is likely that this cross-link involves domain IV. Domain II also makes contact with the 30S subunit (Figs. 3*A* and 4), in the vicinity of proteins S4 and S12 (23), of which the S12 protein is known to form a cross-link with EF-G (7, 25).

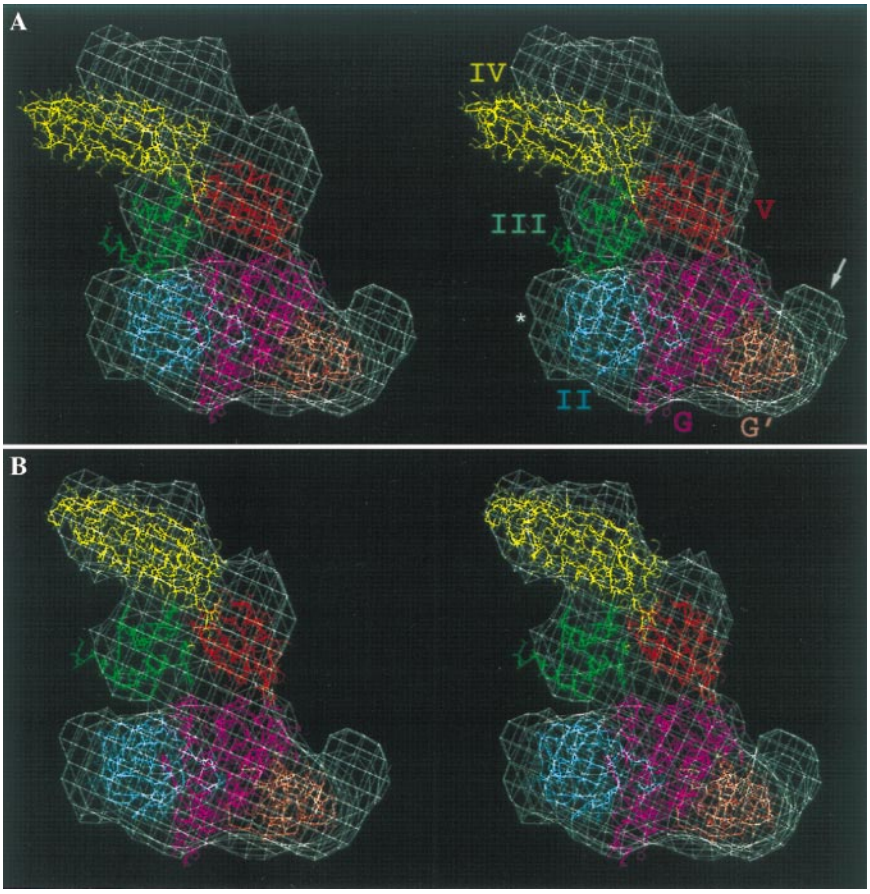

FIG. 2. Stereo view showing the fitting of the crystal structure (9) of EF-G–GDP into the extra mass of density corresponding to EF-G. The density map corresponding to EF-G is shown in white wire-mesh form. The various domains of the crystal structure are shown in different colors. (*A*) Fitting using domains I and II as the main guide to align the whole crystal structure into the density map (see text). (*B*) Separate fitting of the substructure formed by domains III–V (see text). To obtain an optimum fit, this structure was shifted by approximately 10 Å toward the central protuberance of the 50S subunit and rotated by about 10°, around a pivoting point in the contact region between domains II and III, toward the L1 side, whereas domains I and II were left in the same position as in *A*. The arrow points to the portion of the density map that is partially occupied by the G′ domain and involved in making the arc-like connection with the L7/L12 stalk (see also Figs. 1*B* and 3*B*). The asterisk shows a partially unoccupied region that probably comes from the ribosome because of a conformational change at the site of interaction with domain II.

Domain III is in close proximity to a region below the channel and the origin of the platform. Domain II of both EF-G and EF-Tu in the ternary complex appears to make contact with the same region of the 30S subunit (see ref. 24).

The EF-G contact with the 50S subunit, in the region of the L7/L12 stalk base (see Fig. 1*A*), is made through its domains I (core G and insert G′) and V (Figs. 3*A* and 4). The core G domain of EF-G is a structural homolog of the G domain of EF-Tu, which is a conserved feature of the GTPase superfamily (see refs. 9, 10, and 19), whereas the insert portion of domain I of EF-G has no counterpart in EF-Tu (9, 10, 19). The fitting of the x-ray structure reveals that the GDP-binding region of the G domain (9) touches a point at the lower part of the stalk base, whereas the G′ domain connects with a protrusion closer to the stalk, along a thin arc-like structure (Figs. 1*B* and 3*B*). A similar connection seen in the ternary complex was interpreted as a bridge between the C-terminal end of the L7/L12 stalk and the G domain of EF-Tu (24). However, because the stalk is composed of four copies of L7/L12 protein (25), and in our map it is a well-extended separate feature, whose C-terminal domains are located at its tip (25), the arc connection probably involves the C-terminal domain of one of the folded L7/L12 molecules (26).

Domain V, which is important for ribosome binding of EF-G (27), touches and fits into a structurally complementary groove region at the base of the stalk (Figs. 3 and 4). In addition to protein L7/L12, EF-G is known to form cross-links with proteins L6, L14, and L31 (7, 25) present at the base of the stalk. Because the stalk is highly mobile (25, 28) and implicated in both factor binding and translocation (25, 28, 29), its appearance as a well-delineated structure at the moment frozen by fusidic acid binding could indicate that its movement is precisely controlled and choreographed in the course of the translocation process.

The 2,660 loop, one of the universally conserved nucleotide regions of 23S rRNA of the 50S subunit, is the binding site of ribotoxins, α-sarcin and ricin, which abolish all EF-dependent functions of both prokaryotic (30) and eukaryotic (31) ribosomes. Several lines of evidence indicate that this 23S RNA region, along with nucleotides 1,052–1,112 of 23S RNA, of which nucleotides 1,054–1,081 have been cross-linked to EF-G (32), are present near the base of the L7/L12 stalk. Both EF-G and EF-Tu protect some common nucleotides in the 2,660-loop region from chemical modification, whereas EF-G protects additional nucleotides at positions 1,067 (the binding site of the antibiotic thiostrepton) and 1,069 of 23S RNA (33). Protein L11, which is present at the base of the L7/L12 stalk, binds to the region of positions 1,052–1,112 (34) and the pentameric protein complex L10-$(L7/L12)_2$ binds to up- and downstream neighboring regions, positions 1,113–1,124 and 1,028–1,051, of the 23S RNA (35). These results imply that (*i*) the 2,660 region of the 23S RNA is the site where the structurally homologous G domains of both EF-Tu and EF-G interact and (*ii*) the 1,052–1,112 region of the 23S RNA is

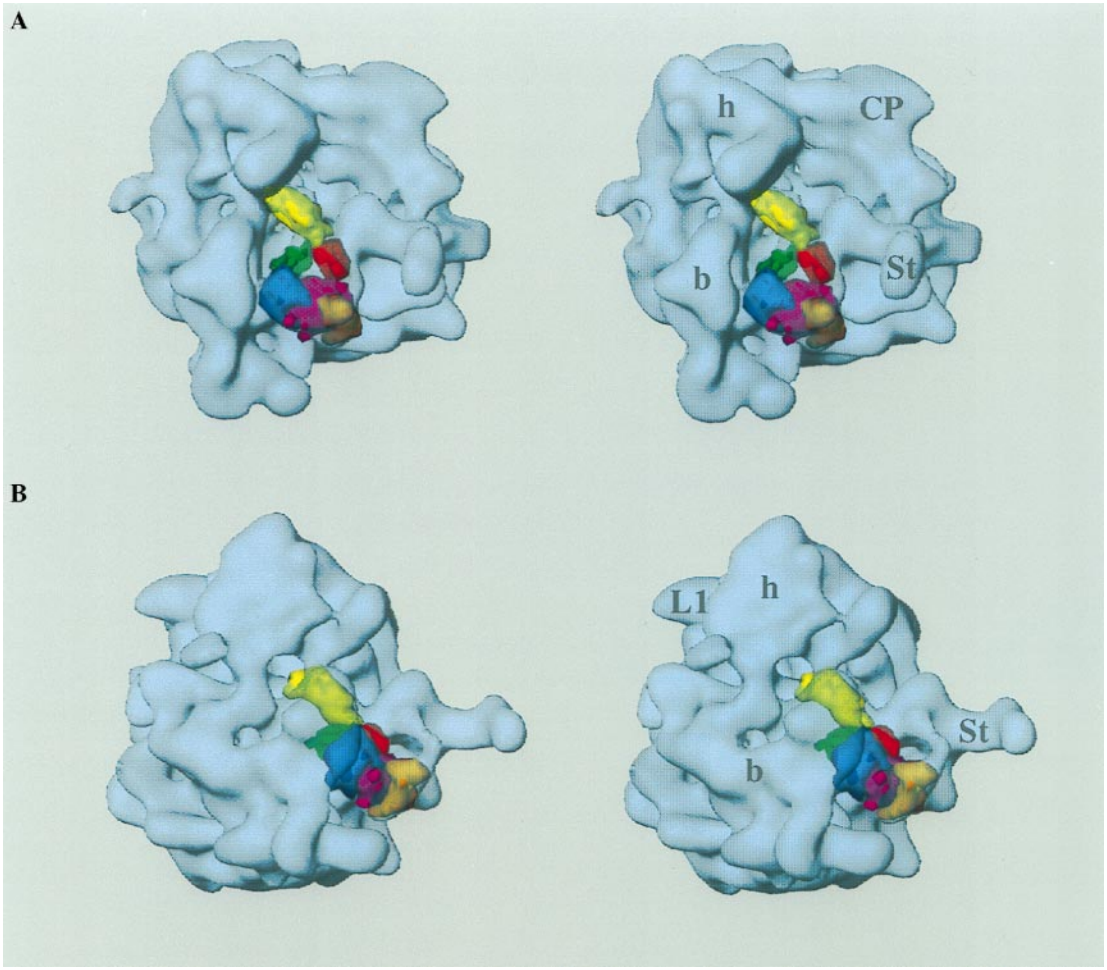

FIG. 3. Stereo view of a low-resolution version of the EF-G x-ray structure shown in Fig. 2*B*, superimposed onto the 3D map of the 70S–EF-G–GDP–fusidic acid complex (shown as a transparent blue surface). Color coding for different domains of the x-ray structure is the same as in Fig. 2: domain I, magenta and brown (core G domain, magenta; insert G′ domain, brown); domain II, blue; domain III, green; domain IV, yellow; and domain V, red. (*A*) In the intersubunit face view, the 30S subunit is on the left and the 50S subunit on the right. (*B*) Same as *a* but presented from the 30S-solvent side to show that the G′ domain is involved in the formation of the arc-like structure with the base of the L7/L12 stalk. Because only the lower part of the arc-like structure is occupied by the x-ray structure, the upper part is probably contributed by the C-terminal domain of one of the folded L7/L12 molecule (see text), which becomes pronounced only upon factor binding (see also ref. 24). Landmarks have been abbreviated to avoid visual complexity of the stereo picture. For 30S subunit: h, head; b, body. For 50S subunit: CP, central protuberance; St, L7/L12 Stalk; L1, L1 protein.

located at a point closer to the stalk, probably where domain V of EF-G interacts with the 50S subunit.

The multiple interactions between the L7/L12 stalk base and domains I and V (Figs. 3 and 4) suggest a complex mechanism of translocation in which these domains may act in concert with the flexible stalk. The stalk may act as an intermediary (see refs. 25, 28, and 29) and effect the movement of domain IV through domain V, which fits into a groove-like

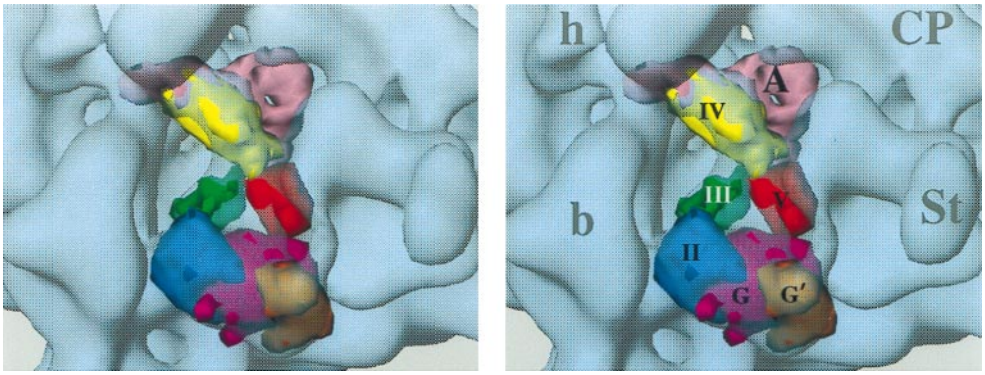

FIG. 4. Same as Fig. 3*A* but showing a magnified view of the site of interaction of different domains of EF-G with the ribosome. Particularly important to note is the partial overlap of domain IV with the A-site tRNA (pink), as obtained from a cryo map of a pretranslocational complex (R.K.A., P.P., R.A.G., N. Burkhardt, R. Jünemann, K. H. Nierhaus, and J.F., unpublished results). Also, note the proximity of the anticodon end of the A site tRNA to the tip of the domain IV. Various domains are labeled with roman numerals and the A-site tRNA is marked as A. Other landmarks are as in Fig. 3.

structure at its base. Moreover, the overlap between the tip of domain IV with the anticodon arm of A-site tRNA (11, 12) (Fig. 4) suggests that this domain displaces the A-site tRNA toward the P-site position by physical interaction with the anticodon arm, i.e., from the L7/L12-stalk side to the L1 protein side (see Figs. 1*B* and 3*C* for structural reference), thereby effecting translocation, as is also suggested from recent nonstructural studies (5, 36).

After completion of this study, the EF-G position on the ribosome was reported, as derived by determining the proximal regions of rRNA to specific amino acids of EF-G by using the hydroxyl radical probing method (37). Even though this study does not throw light on the conformational change of EF-G in the ribosome-bound state, it is in striking agreement with our results, as far as the positions of various EF-G domains and their proximity to specific components of the ribosomal structure (i.e., rRNA segments or ribosomal proteins) are concerned.

We thank Peter Moore for providing the all-atom coordinates of the EF-G–GDP x-ray structure. We thank Yiwei Chen for help in the initial stage of image processing and Amy Heagle for assistance in the preparation of illustrations. We also thank Terence Wagenknecht for critical reading of the manuscript and suggestions. This work was supported by grants from the National Institutes of Health (R37-GM29169 and R01-GM55440) and the National Science Foundation (BIR9219043). Computing support was kindly provided by the National Center for Supercomputer Applications, University of Illinois at Urbana–Champaign.

1. Nishizuka, Y. & Lipmann, F. (1966) *Proc. Natl. Acad. Sci. USA* **55,** 212–219.
2. Kawakita, M., Arai, K. & Kaziro, Y. (1974) *J. Biochem.* **76,** 801–809.
3. Chinali, G. & Parmeggiani, A. (1982) *Eur. J. Biochem.* **125,** 415–421.
4. Voigt, J. & Nagel, K. (1993) *J. Biol. Chem.* **268,** 100–106.
5. Rodnina, M. V., Savelsbergh, A., Katunin, V. I. & Wintermeyer, W. (1997) *Nature (London)* **385,** 37–41.
6. Girshovich, A. S., Kurtskhalia, T. V., Ovchinikov, Y. A. & Vasiliev, V. D. (1981) *FEBS Lett.* **130,** 54–59.
7. Sköld, S. E. (1982) *Eur. J. Biochem.* **127,** 225–229.
8. Willie, G. R., Richman, N., Godtfredson, W. O. & Bodley, J. W. (1975) *Biochemistry* **14,** 1713–1718.
9. Czworkowski, J., Wang, J., Steitz, T. A. & Moore, P. B. (1994) *EMBO J.* **13,** 3661–3668.
10. Al-karadaghi, S., Ævarsson, A., Garber, M., Zheltonosova, J. & Liljas, A. (1996) *Structure* **4,** 555–565.
11. Agrawal, R. K., Penczek, P., Grassucci, R. A., Li, Y., Leith, A., Nierhaus, K. H. & Frank, J. (1996) *Science* **271,** 1000–1002.
12. Stark, H., Orlova, E. V., Rinke-Appel, J., Jünke, N., Mueller, F., Rodnina, M., Wintermeyer, W., Brimacombe, R. & van Heel, M. (1997) *Cell* **88,** 19–28.
13. Burma, D. P., Srivastava, A. K., Srivastava, S. & Dash, D. (1985) *J. Biol. Chem.* **260,** 10517–10525.
14. Lata, K. R., Penczek, P. & Frank, J. (1995) *Ultramicroscopy* **58,** 381–391.
15. Penczek, P., Grassucci, R. A. & Frank, J. (1994) *Ultramicroscopy* **53,** 251–270.
16. Zhu, J., Penczek, P. A., Schröder, R. & Frank, J. (1997) *J. Struct. Biol.* **118,** 197–219.
17. Böttcher, B., Wynne, S. A. & Crowther, R. A. (1997) *Nature (London)* **386,** 88–91.
18. Frank, J., Zhu, J., Penczek, P., Li, Y., Srivastava, S., Verschoor, A., Radermacher, M., Grassucci, R., Lata, R. K. & Agrawal, R. K. (1995) *Nature (London)* **376,** 441–444.
19. Nissen, P., Kjeldgaard, M., Thirup, S., Polekhina, G., Reshetnikova, L., Clark, B. F. C. & Nyborg, J. (1995) *Science* **270,** 1464–1472.
20. Czworkowski, J. & Moore, P. B. (1997) *Biochemistry* **36,** 10327–10334.
21. Johanson, U. & Hughes, D. (1994) *Gene* **143,** 55–59.
22. Abel, K., Yoder, M. D., Hilgenfeld, R. & Jurnak, F. (1996) *Structure* **4,** 1153–1159.
23. Capel, M. S., Engleman, D. M., Freeborn, B. R., Kjeldgaard, M., Langer, J. A., Ramakrishnan, V., Schindler, D. G., Schneider, D. K., Schoenborn, B. P., Sillers, I. -Y., *et al.* (1987) *Science* **238,** 1403–1406.
24. Stark, H., Rodnina, M., Rinke-Appel, J., Brimacombe, R., Wintermeyer, W. & van Heel, M. (1997) *Nature (London)* **389,** 403–406.
25. Traut, R. R., Tewari, D. S., Sommer, A., Govino, G. R., Olson, H. M. & Glitz, D. G. (1986) in *Structure Function and Genetics of Ribosomes*, eds. Hardesty, B. & Kramer, G. (Springer, New York), pp. 286–308.
26. Dey, D., Oleinikov, A. V. & Traut, R. R. (1995) *Biochimie* **77,** 925–930.
27. Hou, Y., Yaskowiak, E. S. & March, P. E. (1994) *J. Bacteriol.* **176,** 7038–7044.
28. Möller, W., Schrier, P. I., Maassen, J. A., Zantema, A., Schop, E., Reinalda, H., Cremers, A. F. M. & Mellema, J. E. (1983) *J. Mol. Biol.* **163,** 553–573.
29. Burma, D. P., Srivastava, S., Srivastava, A. K., Mahanti, S. & Dash, D. (1986) in *Structure Function and Genetics of Ribosomes,* eds. Hardesty, B. & Kramer, G. (Springer, New York), pp. 438–453.
30. Hausner, T.-P., Atmadja, J. & Nierhaus, K. H. (1987) *Biochimie* **169,** 911–923.
31. Wool, I. G., Gluck, A. & Endo, Y. (1992) *Trends Biochem. Sci.* **17,** 266–269.
32. Sköld, S. E. (1983) *Nucleic Acids Res.* **11,** 4923–4932.
33. Moazed, D., Robertson, J. M. & Noller, H. F. (1988) *Nature (London)* **334,** 362–364.
34. Schmidt, F. J., Thompson, J., Lee, K., Dijk, J. & Cundliffe, E. (1981) *J. Biol. Chem.* **266,** 12301–12305.
35. Beauclerk, A. A. D., Cundliffe, E. & Dijk, J. (1984) *J. Biol. Chem.* **259,** 6559–6563.
36. Borowski, C., Rodnina, M. V. & Wintermeyer, W. (1996) *Proc. Natl. Acad. Sci. USA* **93,** 4202–4206.
37. Wilson, K. S. & Noller, H. F. (1998) *Cell* **92,** 131–139.